PAPER • OPEN ACCESS

# Analyses and optimization of the CFETR power conversion system with a new supercritical $CO_2$ Brayton cycle

To cite this article: Pinghui Zhao *et al* 2023 *Nucl. Fusion* **63** 046026

OPEN ACCESS
IOP Publishing | International Atomic Energy Agency
Nuclear Fusion
Nucl. Fusion **63** (2023) 046026 (18pp)
https://doi.org/10.1088/1741-4326/acbe0d

# Analyses and optimization of the CFETR power conversion system with a new supercritical $CO_2$ Brayton cycle

**Pinghui Zhao[1,*], Zhansheng Chen[2], Yixuan Jin[2], Teng Wan[2], Xiaohu Wang[2], Ke Liu[2], Mingzhun Lei[1,*], Yuanjie Li[2] and Changhong Peng[2]**

[1] Institute of Plasma Physics Chinese Academy of Sciences, Hefei 230031, China
[2] School of Nuclear Science and Technology, University of Science and Technology of China, Hefei 230026, China

E-mail: phzhao@mail.ustc.edu.cn and leimz@ipp.ac.cn

Received 20 May 2022, revised 21 December 2022
Accepted for publication 22 February 2023
Published 15 March 2023

**Abstract**

In this paper, the Chinese Fusion Engineering Testing Reactor (CFETR) power conversion system, with a supercritical $CO_2$ ($SCO_2$) Brayton cycle, is designed, analyzed and optimized. Considering the pulse operation of the reactor, a heat storage loop with high temperature molten salt and low temperature concrete is introduced. Based on the parameters of the first cooling loop, the CFETR power conversion loop is designed and studied. A new $SCO_2$ Brayton cycle for the CFETR dual heat sources, blanket and divertor, is developed and optimized using a genetic algorithm. Compared to other simple and recompression cycles, it is shown that the new $SCO_2$ Brayton cycle combines maximum thermal efficiency with simplicity. Exergy analyses are carried out and show that the exergy destruction rates of turbine and heat exchangers between different loops are the largest due to the large turbine power and the large temperature difference. The exergoeconomic analyses show that the fusion reactor accounts for the main cost, which is the key to the economy of fusion power generation. The following sensitivity analyses show that the hot molten salt temperature has a major influence on the system performance. Finally, several multi-criteria optimization algorithms are introduced to simultaneously optimize the three fitness functions, the cycle thermal efficiency, the system exergy efficiency and the total system product unit cost. It is found that the maximum thermal efficiency, the maximum exergy efficiency and the lowest total system product unit cost can be obtained almost simultaneously for the new CFETR power conversion system, and this optimal operation scheme is presented.

Keywords: supercritical $CO_2$ Brayton cycle, CFETR, exergy, exergoeconomic, multi-criteria optimization

(Some figures may appear in colour only in the online journal)

* Authors to whom any correspondence should be addressed.



 

## 1. Introduction

In the face of the increasingly severe energy crisis, the development and utilization of alternative energy has become a new research hot spot. As a sustainable clean energy, fusion energy has great development potential, with advantages including both inherent safety and low environmental impact [1]. International Tokamak Experimental Reactor (ITER), which provides the basis for fusion power generation, is under construction internationally. Developed on the basis of ITER, Chinese Fusion Engineering Testing Reactor (CFETR) is designed to achieve 200–1000 MW fusion power production [2].

Since the $SCO_2$ Brayton cycle has the advantages of a small volume of components, high efficiency under a medium or high temperature heat source, and environmental friendliness, its application in nuclear energy has been widely explored in recent years. Alali and Al-Shboul [3] applied the Brayton cycle in high-temperature gas-cooled reactor studies with air, nitrogen, $SCO_2$ and helium as working media. The results show that the helium cycle has the highest power efficiency and the $SCO_2$ cycle has the highest cogeneration efficiency. Ishiyama *et al* [4] compared the efficiency of the steam Rankine cycle, He Brayton cycle and $SCO_2$ Brayton cycle based on a prototype fusion reactor. It is found that the $SCO_2$ cycle is more efficient than the steam Rankine cycle and has advantages in both system volume and permeated tritium separation. Based on EU DEMO, Stepanek *et al* [5] studied the comparison of several feasible arrangements of the steam Rankine cycle, the He Brayton cycle and the $SCO_2$ Brayton cycle at different heat source temperatures, showing that the $SCO_2$ cycle is competitive in scale complexity, cost and operational flexibility. Linares *et al* [6] compared the thermodynamic characteristics of the He and $SCO_2$ Brayton cycles coupled with other cycles based on the fusion reactor, which shows that the $SCO_2$-$H_2O$ combined cycle has a high efficiency of 46.7%. Bustos Dupre [7] has developed a concept power plant based on a minimal modular reactor and the $SCO_2$ Brayton cycle as a sustainable alternative energy solution for Antarctica. Meanwhile, further detailed thermodynamic and optimization studies on the $SCO_2$ Brayton cycle have been carried out. Kong *et al* [8] proposed a lead based reactor with the $SCO_2$ Brayton power cycle, and its thermodynamic behavior is compared with conventional systems. Wu *et al* [9] developed a thermodynamic analysis solver for efficiency analysis of the $SCO_2$ Brayton simple cycle and recompression cycle in a 100 MW lead-cooled small modular reactor and explored its potential use in dry-cold environments. Syblik *et al* [10] compared the efficiency, power output and other physical parameters of two kinds of $SCO_2$ Brayton cycle. A new computational software for optimizing the cycle was presented and an optimized design of maximizing the power of the fusion plant DEMO was given. Linares *et al* [11–13] conducted a lot of layout and thermodynamic research on the $SCO_2$ cycle with multiple heat sources used in EU DEMO, exploring the optimization scheme. In our previous study [14], the applicability and advantages of the $SCO_2$ Brayton cycle under dual heat sources of CFETR have been proved.

In addition to thermodynamic analysis, exergy economic analysis is also an effective way to study the irreversibility and economy of systems and individual components. Zahedi *et al* [15] aimed at a new configuration including four cycles, analyzing the thermodynamic and economic models of different parts and optimizing the cycle in order to reduce costs and improve exergy efficiency. Wang *et al* [16] proposed a new power conversion system consisting of gas turbine cycle, supercritical carbon dioxide ($SCO_2$) Brayton cycle, organic Rankine cycle and absorption refrigeration cycle, and optimized the performance with exergoeconomic methods. Al-Rashed *et al* [17] proposed an innovative gas turbine-$SCO_2$ cycle, made a comprehensive exergoeconomic analysis and performed multi-criteria optimization to maximize exergy efficiency and minimize power costs. Guelpa *et al* [18] developed an economic analysis method independent of cost functions to optimize the $SCO_2$ Brayton cycle for solar applications. Liu *et al* [19] identified the improvement potential of each important component in the $SCO_2$ Brayton cycle based on advanced economic methods. Du *et al* [20] studied the economic characteristics of the $SCO_2$ Brayton cycle in its full life cycle, and explored the influence of multistage compression and the number of optimal compression stages based on the gas-cooled fast reactor. Luo *et al* [21] established a thermodynamic simulation platform to study the thermodynamic and exergy economic behaviors of six $SCO_2$ Brayton cycles in the fourth generation nuclear reactors, and to optimize the economics of the $SCO_2$ Brayton cycle. Currently, there are few systematic exergoeconomic analyses of the $SCO_2$ Brayton cycle for the fusion energy.

In this paper, based on the CFETR dual heat sources, high temperature blanket and low temperature divertor, several $SCO_2$ Brayton cycles are designed, analyzed and optimized in detail, and finally a new one is proposed. The paper is organized as follows. In section 2, several $SCO_2$ Brayton cycles with dual heat sources are designed. The thermodynamic and exergoeconomic models for the power conversion system are established. In section 3.1, the optimized cycles are compared and the new simple Brayton cycle wins out in terms of cycle efficiency. In sections 3.2 and 3.3, the exergy analyses, the exergoeconomic analyses and the sensitivity analyses for the new $SCO_2$ Brayton cycle are performed. In section 3.4, the multi-criteria optimizations are carried out to show optimal variables and fitness functions. In the final section, conclusions are presented.

## 2. Methodology

A typical schematic diagram of the CFETR power conversion system is shown in figure 1, which mainly comprises the fusion reactor, first cooling loop (FCL), heat storage loop (HSL), power conversion loop (PCL) and sink loop (SL). There are two different heat sources, high-temperature blanket (BNK, 300 °C–500 °C, 70% of total heat) and low-temperature divertor (DIV, 140 °C–200 °C, 30% of total heat) [2] in the FCL. Since CFETR will be in a long-pulse operation with a duty cycle of 0.3–0.5 [22], the HSL is needed to achieve continuous steady-state power generation. The molten salt is chosen for

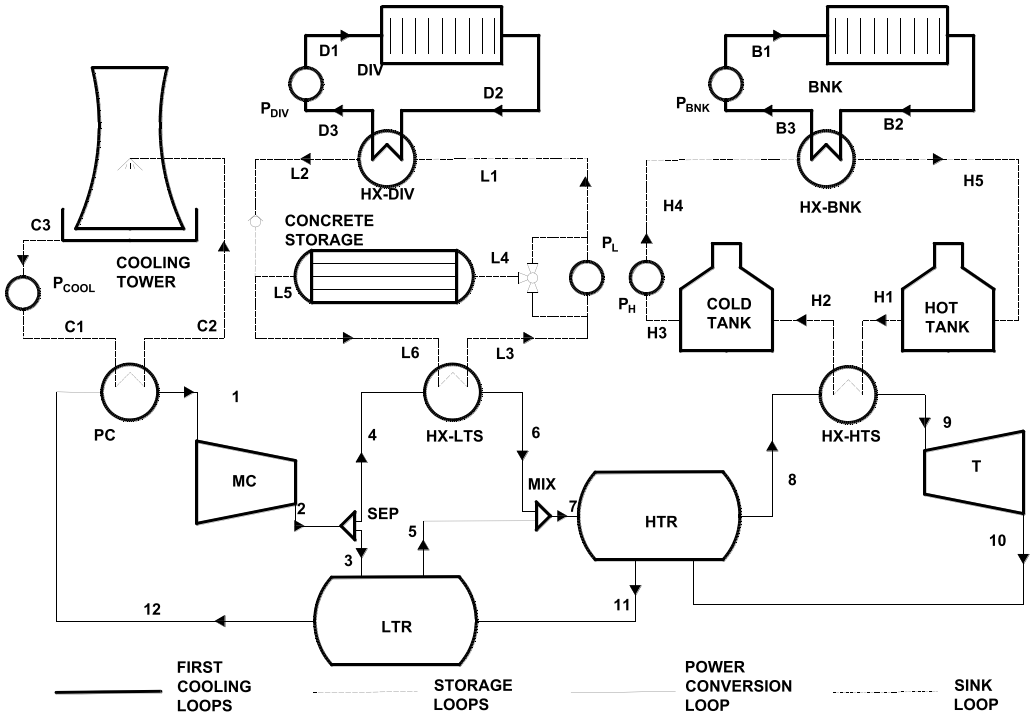


**Figure 1.** Typical schematic diagram of CFETR power conversion system.

**Table 1.** Basic parameters.

| | | | |
|---|---|---|---|
| Heat from BNK | 700 MW[a] | Heat from DIV | 300 MW[a] |
| FCL pressure of BNK | 8 MPa[b] | FCL pressure of DIV | 4.2 MPa[c,d] |
| BNK temperature | 300 °C/500 °C[b] | DIV temperature | 140 °C/200 °C[c,d] |
| Molten salt | 60%$NaNO_3$–40%$KNO_3$[e] | Duty cycle | 0.3–0.5[a,f] |

[a] [2].
[b] [26].
[c] [27].
[d] [28].
[e] [23].
[f] [22].

the heat storage of BNK due to its maturity in solar power generation. However, it is not suitable for DIV heat storage due to the high melting point, 230 °C [23]. Concrete with water or thermal oil may be suitable for medium temperature heat storage. It has benefits such as low cost, easy construction, good mechanical properties, being non-toxic and non-flammable, and has the testing basis and practical applications [24, 25]. Detailed information on FCLs and HSLs are shown in table 1. The PCL of CFETR can choose different $SCO_2$ Brayton cycles, which is very important to the cost of the whole power conversion system. As an example, a simple Brayton cycle with dual heat sources is shown in figure 1. More detailed design and analyses of different $SCO_2$ Brayton cycles for the PCL of CFETR are provided in the later sections of the paper. In addition, the meanings of abbreviations and symbols are shown in table A1.

### 2.1. $SCO_2$ Brayton cycle configurations

In view of the special dual heat sources of the fusion reactor, several $SCO_2$ Brayton cycle configurations with different heat source arrangements are designed in this paper, as shown in figures 2(*a*)–(*f*). $SCO_2$ Brayton cycles mainly consist of the heat exchanger between the molten salt storage loop and the $SCO_2$ Brayton cycle HX-HTS, the heat exchanger between the concrete storage loop and the $SCO_2$ Brayton cycle HX-LTS, the heat exchanger between the $SCO_2$ Brayton cycle and the sink loop PC, the high/low temperature recuperator HTR/LTR, the compressor MC (main compressor), the auxiliary compressor AC, the turbine T, the separator SEP and the mixer MIX.

There are two main types of $SCO_2$ Brayton cycle, the simple cycle and the recompression cycle. In previous research [29, 30], the recompression cycle is usually more efficient and economical than the simple cycle for the single heat source. Figure 2(*a*) shows a simple cycle configuration with only the blanket heat source, and figure 2(*b*) shows a recompression cycle configuration with only the blanket heat source. To improve the thermal efficiency, the low temperature divertor heat source needs to be added reasonably. Since the specific heat capacity of $SCO_2$ on the high-pressure side of the recuperator is much higher than that on the low-pressure side, the flow split method, with a fraction of the high-pressure $CO_2$ entering the LTR, is adopted. And thus, the temperature

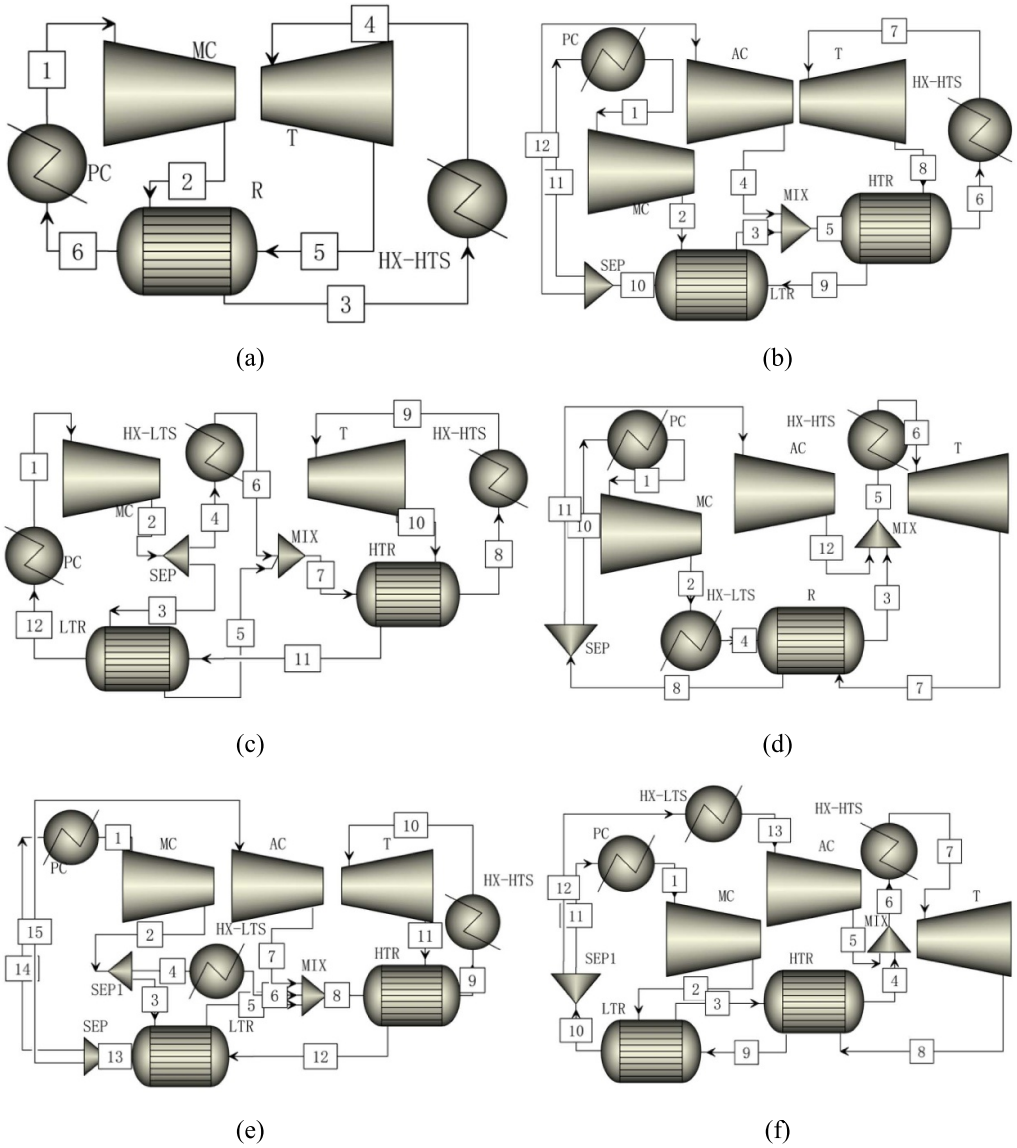


**Figure 2.** $SCO_2$ Brayton cycle configurations: (*a*) simple cycle with single heat source, (*b*) recompression cycle with single heat source, (*c*) simple cycle with dual heat sources, (*d*) recompression cycle with dual heat sources 1, (*e*) recompression cycle with dual heat sources 2 and (*f*) recompression cycle with dual heat sources 3.

difference of the recuperator on the high-pressure side can be reduced and the heat recovery increases, which is the main reason for improving the heat efficiency of the recompression cycle. Based on this idea, we add the divertor heat source to the high pressure $SCO_2$ side, and design the simple or recompression cycles for the CFETR dual heat sources as shown in figures 2(*c*)–(*f*).

Figure 2(*c*) is based on the simple Brayton cycle, where the DIV heat source is arranged in parallel with the LTR. Figures 2(*d*)–(*f*) are based on the recompression Brayton cycles. In figure 2(*d*), the DIV heat source is used to replace the low-temperature recuperator. In figure 2(*e*), the DIV heat source, AC and LTR are connected in parallel. In figure 2(*f*), the DIV is connected in series before the AC, the outflow of which enters the main stream after the HTR. To better perform the cycle thermodynamic analysis, figure 3 gives the *T*–*s* diagram corresponding to figures 2(*c*) and (*e*).

### 2.2. Thermodynamics analysis

In this section, the energy and exergy models of each component are established. For a single component, the energy balance equation is:

$$\sum_{\text{in}} q_{\text{in}} \cdot h_{\text{in}} + \sum Q = \sum_{\text{out}} q_{\text{out}} \cdot h_{\text{out}} + \sum W \tag{1}$$

where $q_{\text{in}}/q_{\text{out}}$ is the mass flow rate, $h_{\text{in}}/h_{\text{out}}$ denotes the enthalpy of the component at inlet and outlet, $Q$ is the input heat flow and $W$ is the output work.

The expression of turbine work can be obtained from the above general expression:

$$W_{\text{T}} = \left(h_{\text{T,in}}\left(p_{\text{T,in}}, T_{\text{T,in}}\right) - h_{\text{T,out}}\left(p_{\text{T,out}}, T_{\text{T,out}}\right)\right) \cdot q_{\text{T}} \cdot \varepsilon_{\text{T}}. \tag{2}$$

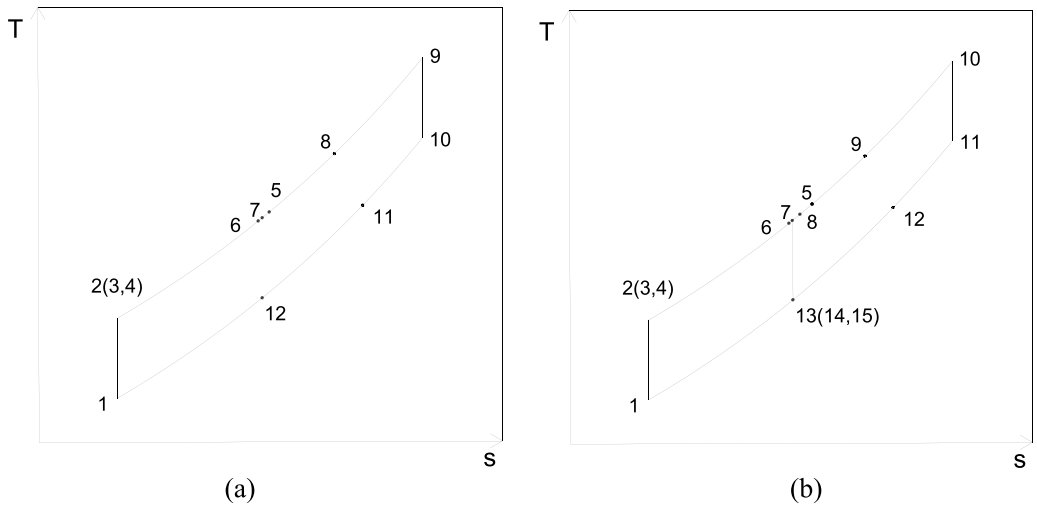


**Figure 3.** *T*–*s* diagram: (*a*) simple Brayton cycle with dual heat sources, (*b*) recompression Brayton cycle with dual heat sources 2.

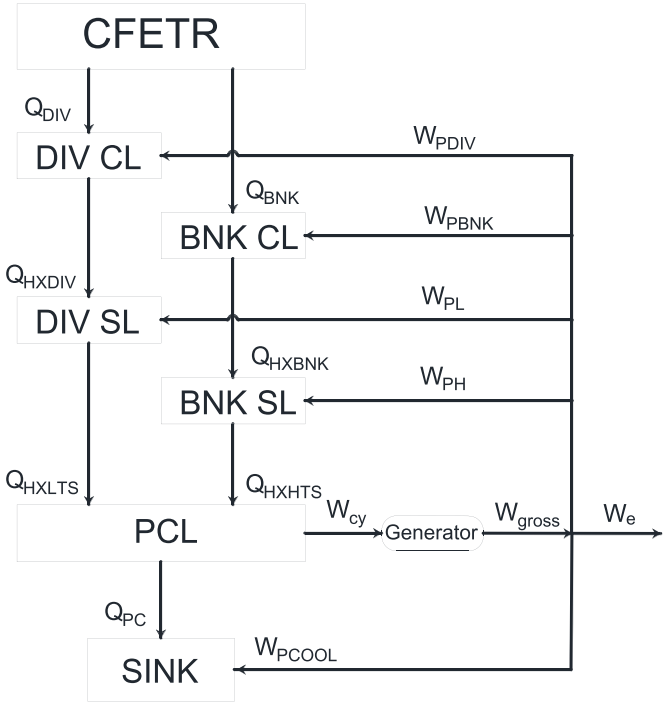


**Figure 4.** Energy conversion diagram in the fusion system.

The work consumption terms in the system, namely the work of the compressor and the pump, are expressed as:

$$W_{\mathrm{c}} = \left(h_{\mathrm{c,out}}\left(p_{\mathrm{c,out}}, T_{\mathrm{c,out}}\right) - h_{\mathrm{c,in}}\left(p_{\mathrm{c,in}}, T_{\mathrm{c,in}}\right)\right) \cdot q_{\mathrm{c}}/\varepsilon_{\mathrm{c}} \quad (3)$$

$$W_{\mathrm{p}} = \left(h_{\mathrm{p,out}}\left(p_{\mathrm{p,out}}, T_{\mathrm{p,out}}\right) - h_{\mathrm{p,in}}\left(p_{\mathrm{p,in}}, T_{\mathrm{p,in}}\right)\right) \cdot q_{\mathrm{p}}/\varepsilon_{\mathrm{p}}. \quad (4)$$

Figure 4 shows the energy conversion diagram in the fusion system, in which $W_{\mathrm{cy}}$ is the network of the PCL, $W_{\mathrm{cy}} = W_{\mathrm{T}} - W_{\mathrm{c}}$, $W_{\mathrm{gross}}$ is the generating capacity of the generator, $W_{\mathrm{gross}} = \kappa_{\mathrm{ele}} * W_{\mathrm{cy}}$, and $W_{\mathrm{e}}$ is the net electricity power after subtracting the pump work of the first loop, HSL and SL (the electricity consumed by the system itself):

$$W_{\mathrm{e}} = \kappa_{\mathrm{ele}} * (W_{\mathrm{T}} - W_{\mathrm{c}}) - W_{\mathrm{pBNK}} - W_{\mathrm{pDIV}} - W_{\mathrm{pL}} - W_{\mathrm{pH}} - W_{\mathrm{pCOOL}}. \quad (5)$$

The detailed equations for these kinds of work are shown in table A2. The ratios of the above work to the total heat of the system are respectively defined as the PCL thermal efficiency $\eta_{\mathrm{cy}}$, the gross efficiency $\eta_{\mathrm{gross}}$ and the electrical efficiency $\eta_{\mathrm{e}}$. However, considering the CFETR long pulse with the duration working time parameter 0.3–0.5 [22], one 2 h periodic plasma pulse consists of 50 min flattop burning and 70 min dwell times [22]. The three efficiency calculation equations are defined as:

$$\eta_{\mathrm{cy}} = \frac{12 * (W_{\mathrm{T}} - W_{\mathrm{c}})}{5 * (Q_{\mathrm{BNK}} + Q_{\mathrm{DIV}})} \tag{6}$$

$$\eta_{\mathrm{gross}} = \frac{12 * ((W_{\mathrm{T}} - W_{\mathrm{c}}) \cdot \kappa_{\mathrm{ele}})}{5 * (Q_{\mathrm{BNK}} + Q_{\mathrm{DIV}})} \tag{7}$$

$$\eta_{\mathrm{e}} = \frac{12 * ((W_{\mathrm{T}} - W_{\mathrm{c}}) \cdot \kappa_{\mathrm{ele}} - W_{\mathrm{pCOOL}} - W_{\mathrm{pL}} - W_{\mathrm{pH}}) - 5 * (W_{\mathrm{pBNK}} + W_{\mathrm{pDIV}})}{5 * (Q_{\mathrm{BNK}} + Q_{\mathrm{DIV}})}. \tag{8}$$

In the absence of the effects of nuclear, electrical, and chemical reaction, as well as magnetic and surface tension, only the changes in the physical exergy of the working medium are considered [31]. Ignoring kinetic and potential exergies, the physical exergy of the working media is expressed as:

$$e = (h - h_0) - T_0 (s - s_0). \tag{9}$$

For each component, the exergy balance is expressed as:

$$\sum_{\mathrm{in}} q_{\mathrm{in}} \cdot e_{\mathrm{in}} + \sum_{j} E_{\mathrm{q,j}} = \sum_{\mathrm{out}} q_{\mathrm{out}} \cdot e_{\mathrm{out}} + \sum W + E_{\mathrm{d}} \tag{10}$$

where $E_{\mathrm{d}}$ denotes the exergy destruction rate in the control volume. $E_{\mathrm{q},j}$ denotes the maximum amount of work that can be converted from the heat $\delta Q_{\mathrm{q},j}$ under ambient conditions, and is calculated as follows:

$$E_{\mathrm{q},j} = \int \delta Q_{\mathrm{q},j} \left(1 - \frac{T_0}{T_{\mathrm{q},j}}\right). \tag{11}$$

The system exergy efficiency is calculated as:

$$\eta_{\mathrm{ex}} = \frac{12 * ((W_{\mathrm{T}} - W_{\mathrm{c}}) \cdot \kappa_{\mathrm{ele}} - W_{\mathrm{pCOOL}} - W_{\mathrm{pL}} - W_{\mathrm{pH}}) - 5 * (W_{\mathrm{pBNK}} + W_{\mathrm{pDIV}})}{5 * (E_{\mathrm{qbnk}} + E_{\mathrm{qdiv}})}. \tag{12}$$

### 2.3. Exergoeconomic analysis

For each component in the system, the exergoeconomic model is established based on the specific exergy costing (SPECO) method [32]. Exergoeconomic models are used to define and calculate the unit cost of the product flow by revealing the cost formation process. The general cost balance equation for each component in the system is expressed as:

$$\sum C_{\mathrm{out},k} + \sum C_{\mathrm{w},k} = \sum C_{\mathrm{in},k} + \sum C_{\mathrm{q},k} + Z_k \tag{13}$$

where $C_{\mathrm{in},k}$ and $C_{\mathrm{out},k}$ denote the cost rates associated with the inlet and outlet exergy streams respectively (\$ $\mathrm{h}^{-1}$), and $C_{\mathrm{w},k}$ and $C_{\mathrm{q},k}$ denote the cost rates associated with the component output power and the input energy (\$ $\mathrm{h}^{-1}$) respectively. The term $Z_k$ is the cost rate associated with the capital investment, operation and maintenance expenses for the $k$th component (\$ $\mathrm{h}^{-1}$). Moreover, accounting for inflation, $Z_k$ has been corrected to a reference year (2021) value as follows:

$$Z_k = \frac{\mathrm{CEPCI}_{2021}}{\mathrm{CEPCI}_{\mathrm{base}}} \times \frac{\mathrm{CRF} \times (1 + \phi)}{\tau} \times \mathrm{PEC}_k \tag{14}$$

$$\mathrm{CRF} = \frac{i(1+i)^n}{(1+i)^n - 1} \tag{15}$$

where CEPCI is the chemical engineering plant cost index, CRF is the capital recovery factor, $\phi = 0.06$ is the maintenance factor, $\tau = 8000$ h is the annual operating hours, $i = 10\%$ is the interest rate, $n = 20$ is the number of operation years [21, 33, 34], and PEC is the purchased-equipment cost. The detailed cost functions for the exergoeconomic analysis are presented in table 2.

Once the cost rate for each flow in the system is obtained, fuel and product-related cost rates can be defined for each component based on the fuel-product-loss principle [31] for further component-based analyses. The specific costs of fuel and product for each component of the system can be defined by the following equations:

$$c_{\mathrm{F},k} = C_{\mathrm{F},k} / E_{\mathrm{F},k} \tag{16}$$

$$c_{\mathrm{P},k} = C_{\mathrm{P},k} / E_{\mathrm{P},k}. \tag{17}$$

For the component analyses, the exergy destruction ($C_{\mathrm{d},k}$ (\$ $\mathrm{h}^{-1}$)), the relative cost difference ($r_k$), and the exergoeconomic factor ($f_k$) of the $k$th component are defined as:

$$C_{\mathrm{d},k} = c_{\mathrm{F},k} \cdot E_{\mathrm{d},k} \tag{18}$$

$$r_k = (c_{\mathrm{P},k} - c_{\mathrm{F},k}) / c_{\mathrm{F},k} \tag{19}$$

$$f_k = Z_k / (Z_k + C_{\mathrm{d},k}). \tag{20}$$

**Table 2.** The capital investment cost function of system components.

| Component | Capital investment cost function ($) | Year (CEPCI) |
|---|---|---|
| BNK[a,b] | 941.6 M$ | 1990 |
| DIV[a,b] | 235.4 M$ | 1990 |
| Fuel[c] | $6\ \$\ (\mathrm{MWh})^{-1}$ | 1988 |
| Turbine[d] | $\frac{479.34q}{0.93-\eta_T}\ln\left(\frac{p_{in}}{p_{out}}\right)(1+\exp(0.036T_{in}-54.4))$ | 1996 |
| Compressor[d] | $\frac{71.1q}{0.9-\eta_c}\cdot\frac{p_{out}}{p_{in}}\ln\left(\frac{p_{out}}{p_{in}}\right)$ | 1996 |
| HTR, LTR, HX-LTS, HX-BNK[e] | $2681*A_k^{0.59}$ | 1986 |
| PC, IC[e] | $2143*A_k^{0.514}$ | 1986 |
| Pump[e] | $1120*W_p^{0.8}$ | |
| HOT TANK[f] | $50\%\cdot 24\cdot Q\cdot\frac{284}{T_{salt1}-T_{salt2}}$ | |
| COLD TANK[f] | $50\%\cdot 6.696\cdot 10^7\cdot\left(\frac{284}{T_{salt1}-T_{salt2}}\cdot\frac{Q}{2.79\cdot 10^3}\right)^{0.8}$ | |

[a] [35].
[b] [36].
[c] [37].
[d] [21].
[e] [33].
[f] [34].

For the exergoeconomic performance evaluation of the overall system, the total system product unit cost ($cp_{tot}$) is calculated as:

$$cp_{tot}=\frac{5}{12}\cdot\frac{\sum_{k=1}^{NK}Z_k+C_{fuel}}{\sum_{i=1}^{NP}E_{P,i}} \tag{21}$$

where $C_{fuel}$ is the fuel cost of the system ($\$\ h^{-1}$), $E_{P,i}$ is the output exergy of each component; the detailed calculations can be seen in table A4 . $NK$ is the number of all components in the system and $NP$ is the number of work components.

### 2.4. Optimization algorithm

In this study, the CFETR power conversion system is optimized by the brute force (BF) algorithm [38] and the genetic algorithm (GA) [39]. The BF algorithm is one of the simplest and most direct methods, which requires a lot of computation, but can guarantee the acquisition of global variables. With the BF algorithm, the parameter interval is first sliced, and then parameters are permutated and combined to calculate all the fitness functions. The fitness function is compared one by one, until the best value is found. GA is a random global search method based on the Darwinian survival of the fittest principle, which randomly generates the initial population, defines the fitness function, and then improves it by repeated application of mutation cross inversion and selection operator [39]. In the process of searching evolution, only the fitness function is used as the basis of genetic operation to evaluate the merits of individuals or solutions. The GA has been applied to optimize various power conversion cycles [40–42]. At present, hot molten salt temperature $T_{H1}$, split ratio of PCL, MC outlet pressure $p_H$ and MC inlet pressure $p_L$ are selected as optimization variables. Fitness functions are the PCL thermal efficiency, the system exergy efficiency and the total system product unit cost. Then the optimization problem can be expressed as follows:

Maximum $\eta_{cy}(T_{H1},\mathrm{sep},p_H,p_L)$
Maximum $\eta_{ex}(T_{H1},\mathrm{sep},p_H,p_L)$
Minimum $cp_{tot}(T_{H1},\mathrm{sep},p_H,p_L)$
Subjected to:

$$\begin{cases}355\leqslant T_{H1}\leqslant 485\,(^\circ\mathrm{C})\\ 0.1\leqslant \mathrm{sep}\leqslant 0.9\\ 15\leqslant p_H\leqslant 30\,(\mathrm{MPa})\\ 7.38\leqslant p_L\leqslant 12\,(\mathrm{MPa})\,.\end{cases} \tag{22}$$

Considering the material processing restrictions [30, 43], the optimization parameter ranges are changed partly:

$$\begin{cases}355\leqslant T_{H1}\leqslant 485\,(^\circ\mathrm{C})\\ 0.1\leqslant \mathrm{sep}\leqslant 0.9\\ 15\leqslant p_H\leqslant 23.3\,(\mathrm{MPa})\\ 7.69\leqslant p_L\leqslant 12\,(\mathrm{MPa})\end{cases}. \tag{23}$$

Based on the GA, the multi-criteria optimizations, Pareto front [41] and method of weighting [44], are used to show the optimal results of the three fitness functions. The Pareto front is to obtain the set of all optimal solutions under multiple fitness functions. The method of weighting is developed by introducing a new fitness function by weighting coefficients before multiple fitness functions. In method of weighting, the three fitness functions are first normalized according to equation (24). Then the multi-criteria function is defined as equation (25) assumed that the three fitness functions have the same importance. A detailed introduction can be referred to [41, 45]. The basic parameters of the GA are shown in table 3.

$$\bar{X}=\frac{X-X_{min}}{X_{max}-X_{min}} \tag{24}$$

$$f=\frac{1}{3}*\bar{\eta}_{cy}+\frac{1}{3}*\bar{\eta}_{ex}+\frac{1}{3}*(1-\overline{cp}_{tot})\,. \tag{25}$$

**Table 3.** Parameters of GA for the present study [17, 42, 46].

| | |
|---|---|
| Population size | 1600 |
| Crossover probability | 0.8 |
| Mutation probability | 0.2 |
| Elite count | 20 |
| Stop generation | 500 |

### 2.5. Validation of modeling and optimization methods

The detailed thermodynamic and exergoeconomic models of the whole CFETR power conversion system are programmed with Python. The detailed exergy and exergoeconomic equilibrium equations are as shown in table A5. The minimum temperature difference between cold and hot fluids in the heat exchanger between different loops is set as 15 °C [34]. The minimum temperature difference for the printed circuit heat exchanger (PCHE) is set as 5 °C [13]. According to the [11, 47], it is assumed that the pressure drops of blanket and divertor are 0.5 and 0.25 MPa, and the pressure drops of the heat exchangers in HSL, in PCL and in SL are 0.06, 0.04 and 0.2 MPa, respectively. The isentropic efficiency is set as 0.92 and 0.88 for turbine and compressor [13]. The isentropic efficiency of pump/compressor is assumed to be 0.85, 0.82 and 0.85 respectively based on the working medium water, helium and molten salt [13, 23]. The generator efficiency is assumed to be 97% [23].

The main program is used to solve the thermophysical properties of each product flow in the system according to the key input variables. Then the cost balance equations of each loop are solved simultaneously. Finally, the efficiency and the cost per unit of electricity are calculated. According to the minimum heat transfer temperature difference requirements, the following constraints should be satisfied: HX-LTS inlet temperature <110 °C, outlet temperature <170 °C, and HX-HTS inlet temperature <270 °C and >230 °C, outlet temperature <470 °C. The program logic and constraints are detailed in the figure 5. In the simulation, the thermal properties of $SCO_2$, water and helium are obtained using REFPROP, and the molten salt of the heat storage system is 60%$NaNO_3$–40%$KNO_3$, with its main thermal properties based on [48].

To validate the accuracy of our models, the efficiency of both the simple and recompression Brayton cycles are compared to those in [13, 23]. The detailed results are shown in table A3, which is basically consistent with the literature [13, 23].

The BF algorithm is implemented by calling library functions scipy.optimize [49], and GA is implemented by Geatpy [50] in python. The results are verified by comparison to the published data in [42]. The validation results are shown in the table 4, and the optimization results are in good agreement with the literature [42].

## 3. Results and discussion

In this section, the most suitable $SCO_2$ Brayton cycle configuration for dual heat sources is firstly obtained by analyzing the optimized thermal efficiency. Then, the exergy analysis, exergoeconomic analysis, and sensitivity analyses for the new $SCO_2$ Brayton cycle are carried out. The effect of the key variables on the cycle thermal efficiency, system exergy efficiency and total system product unit cost is studied. Finally, the methods of multi-criteria optimization are explored and the appropriate optimization scheme is proposed.

### 3.1. $SCO_2$ Brayton cycle configuration analysis

For the six cycles in figure 2, the optimizations based on thermal efficiency $\eta_{cy}$ by GA are carried out. The thermal efficiency here is calculated by equation (6). The optimal efficiency and corresponding variables are given in table 5. It can be seen that when only the BNK is considered, the recompression cycle does have advantage to the simple cycle. But for the dual heat sources, the simple cycle in figure 2(*c*) has the best performance. The use of the DIV heat source and the recompressor can both solve the problem of imbalance between the cold and hot side of heat exchanger caused by the drastic change of $SCO_2$ properties. For dual heat sources, the recompression arrangements make the DIV heat source underutilized, so the efficiency is lower than that of the simple cycle. The cycle efficiency of figures 2(*d*) and (*f*) is even lower than that of figure 2(*e*), which may be caused by the waste of regenerative heat.

To sum up, the dual heat source Brayton cycle in figure 2(*c*) is the best choice for the CFETR power conversion system due to its simplicity and high thermal efficiency. In sections 3.2–3.4, this new $SCO_2$ Brayton cycle with dual heat sources will be further studied and optimized by thermodynamic, exergy and exergoeconomic analyses.

### 3.2. Thermodynamic, exergy and exergoeconomic analyses

For the new $SCO_2$ Brayton cycle with dual heat sources for CFETR, corresponding to the maximum cycle efficiency, detailed fitness functions and variables are shown in table 6. It can be seen that the optimal hot molten salt temperature is around 438.2 °C, the split ratio is 0.64, the MC outlet pressure is about 24.5 MPa, the MC inlet pressure is 7.9 MPa, the maximum cycle thermal efficiency is 37.4%, the system exergy efficiency is 59.8%, and the total system product unit cost is 49.64 \$ $GJ^{-1}$.

The temperature, pressure, mass flow rate, enthalpy, entropy, exergy and cost of each product flow for the new cycle at maximum efficiency are listed in table 7. The exergy and cost for individual components are listed in table 8. The main data in table 7 are collated and plotted for the following analyses.

Figure 6(*a*) is the histogram of the exergy destruction rate and the exergy destruction ratio of each component. The exergy destruction in the fusion reactor is the largest, accounting for nearly 33% of the entire system, for that there is a large difference between the cooling medium inlet temperature and BNK/DIV temperature. Secondly, the exergy destruction rates in the heat exchangers between the first loop and second loop are also very large. As shown in table 7, the temperature of

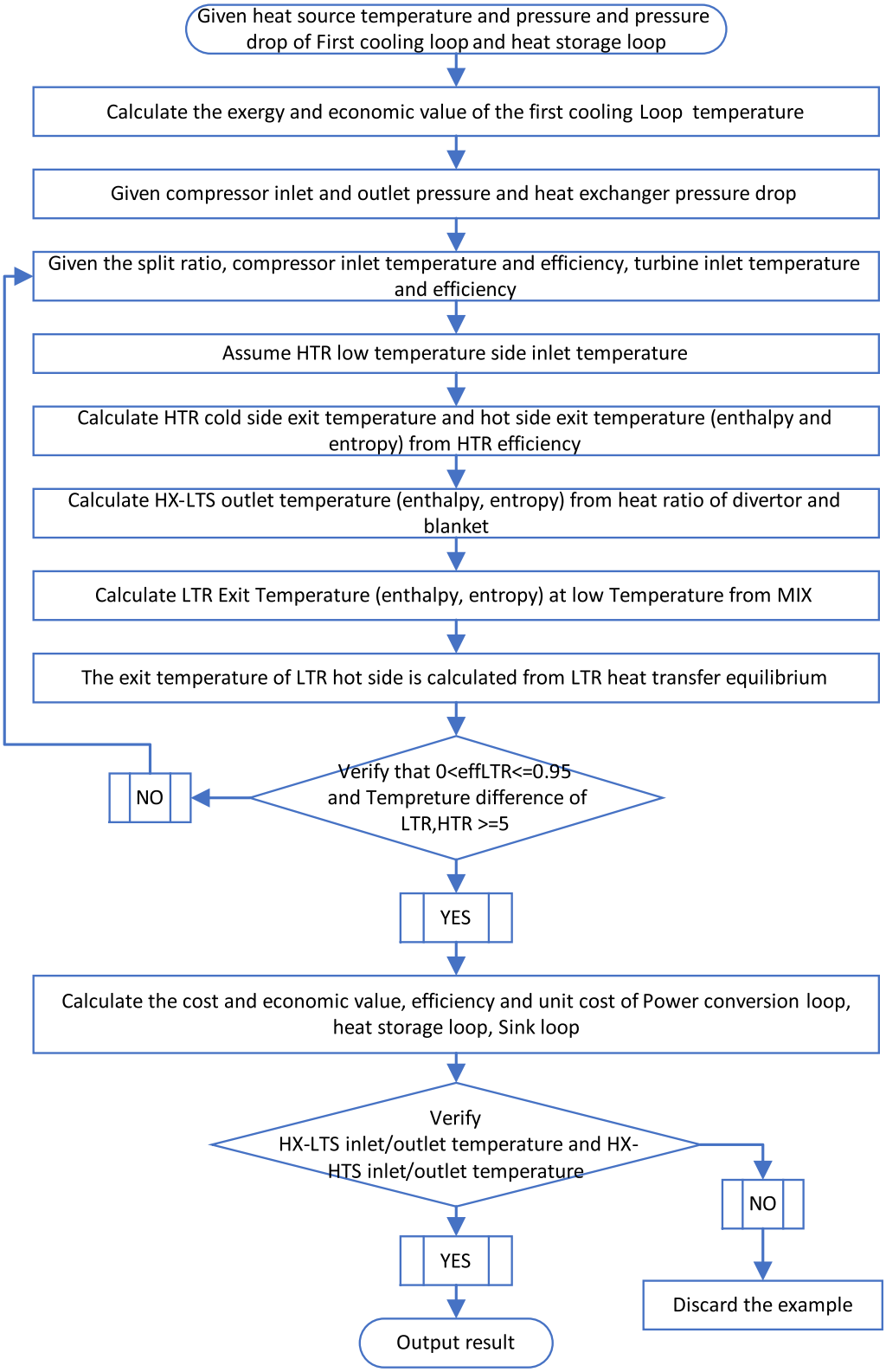


**Figure 5.** Scheme of main program.

the HSL is determined by the PCL, and the maximum temperature difference between the HSL and the FCL can reach more than 50 °C. In the PCL, the exergy destruction of the turbine is large, and further improvement of the turbine efficiency can reduce the exergy destruction. Since the PCHE recuperators have very good heat transfer performance, they have less exergy destruction than heat exchangers between loops. Figure 6(*b*) shows the pie chart of the exergy destruction of

**Table 4.** Comparison of the optimization results between the present study and [42].

| | | | | SR | | PR | | Efficiency (%) | |
|---|---|---|---|---|---|---|---|---|---|
| $T_H$ (°C) | $T_L$ (°C) | $e_{HTR}$ (%) | $e_{LTR}$ (%) | Ref. | Val. | Ref. | Val. | Ref. | Val. |
| 700 | 45 | 97 | 88 | 0.7 | 0.7 | 2.67 | 2.67 | 52.2 | 52.18 |

**Table 5.** Comparison of optimal Brayton cycle efficiency.

| Cycle | Source | Figure 2 | HT (°C) | HP (MPa) | LP (MPa) | SEP | SEP1 | Efficiency |
|---|---|---|---|---|---|---|---|---|
| Simple | BNK | (*a*) | 485.0 | 30.0 | 9.3 | — | — | 29.6% |
| Recompression | BNK | (*b*) | 452.2 | 29.9 | 8.3 | 0.69 | — | 32.1% |
| Simple | BNK + DIV | (*c*) | 438.2 | 24.5 | 7.9 | 0.64 | — | 37.4% |
| Recompression | BNK + DIV | (*d*) | 436.1 | 28.4 | 7.7 | 0.76 | — | 32.7% |
| Recompression | BNK + DIV | (*e*) | 454.8 | 26.1 | 7.8 | 0.92 | 0.74 | 34.8% |
| Recompression | BNK + DIV | (*f*) | 431.2 | 29.7 | 8.0 | 0.75 | — | 31.7% |

**Table 6.** Optimization results for the CFETR power conversion system.

| | Optimization results | | | | | | | | |
|---|---|---|---|---|---|---|---|---|---|
| Cycle | $T_{H1}$ (°C) | Sep | $p_H$ (MPa) | $p_L$ (MPa) | $T_{L6}$ (°C) | $T_{H2}$ (°C) | $\eta_{gross}$ | $\eta_{ex}$ | $cp_{tot}$ ($ GJ$^{-1}$) |
| Simple (BNK + DIV) | 438.2 | 0.64 | 24.5 | 7.9 | 184.6 | 285.0 | 37.4% | 59.8% | 49.64 |

**Table 7.** Thermodynamic properties of the CFETR power conversion system.

| Stream | $P$ (MPa) | $T$ (°C) | $Q$ (kg s$^{-1}$) | $H$ (kJ kg$^{-1}$) | $S$ (kJ /(kg·K) $^{-1}$) | $E$ (MW$^{-1}$) | $C$ ($ h$^{-1}$) |
|---|---|---|---|---|---|---|---|
| H1 | 0.1 | 438.2 | 3198.8 | 625.3 | 1.4 | 540.5 | 131 968.2 |
| H2 | 0.1 | 285.0 | 3198.8 | 384.4 | 1.1 | 344.8 | 84 189.2 |
| H3 | 0.1 | 285.0 | 1370.9 | 384.4 | 1.1 | 827.5 | 84 673.8 |
| H4 | 0.1 | 285.0 | 1370.9 | 384.4 | 1.1 | 827.5 | 84 673.8 |
| H5 | 0.1 | 438.2 | 1370.9 | 625.3 | 1.4 | 1297.1 | 131 403.4 |
| L1 | 3.0 | 80.1 | 672.7 | 337.3 | 1.1 | 20.0 | 3658.8 |
| L2 | 3.0 | 184.6 | 672.7 | 784.3 | 2.2 | 0.1 | 15 321.1 |
| L3 | 2.9 | 80.1 | 288.3 | 337.3 | 1.1 | 8.3 | 2881.1 |
| L4 | 2.9 | 80.1 | 384.4 | 337.3 | 1.1 | 0.0 | 777.7 |
| L5 | 3.0 | 184.6 | 384.4 | 784.3 | 2.2 | 0.1 | 8755.0 |
| L6 | 3.0 | 184.6 | 288.3 | 784.3 | 2.2 | 44.1 | 6566.1 |
| 1 | 7.9 | 32.0 | 1658.1 | 300.6 | 1.3 | 334.6 | 490 098.4 |
| 2 | 24.5 | 65.1 | 1658.1 | 327.1 | 1.3 | 374.1 | 491 574.6 |
| 3 | 24.5 | 65.1 | 1003.6 | 327.1 | 1.3 | 240.3 | 315 715.6 |
| 4 | 24.5 | 65.1 | 564.5 | 327.1 | 1.3 | 133.8 | 175 859.0 |
| 5 | 24.4 | 173.2 | 1003.6 | 543.8 | 1.9 | 298.8 | 405 556.8 |
| 6 | 24.4 | 169.6 | 564.5 | 538.1 | 1.9 | 165.2 | 188 325.8 |
| 7 | 24.4 | 171.9 | 1658.1 | 541.7 | 1.9 | 464.0 | 593 882.6 |
| 8 | 24.4 | 270.0 | 1658.1 | 680.6 | 2.2 | 559.0 | 741 348.5 |
| 9 | 24.3 | 423.2 | 1658.1 | 874.2 | 2.5 | 729.7 | 789 174.2 |
| 10 | 8.0 | 300.9 | 1658.1 | 753.8 | 2.5 | 521.2 | 763 436.5 |
| 11 | 8.0 | 178.2 | 1658.1 | 614.9 | 2.2 | 420.6 | 616 044.1 |
| 12 | 7.9 | 69.4 | 1658.1 | 475.8 | 1.9 | 359.3 | 526 276.5 |
| C1 | 0.2 | 15.0 | 1764.9 | 63.2 | 0.2 | 0.2 | 6.8 |
| C2 | 0.1 | 54.4 | 1764.9 | 227.8 | 0.8 | 18.2 | 36 201.5 |
| C3 | 0.1 | 15.0 | 1764.9 | 63.1 | 0.2 | 0.0 | 1.2 |

each loop in the system, where the reactor, HSLs and PCL all have relatively large exergy destruction. There are a few components in the SL and FCLs, and the heat transfer temperature difference between the SL and the PCL is small, so the SL and the FCLs have relatively low exergy destruction rates.

Figure 7(*a*) shows the fixed investment and maintenance costs and their ratios for different components. The costs are mainly from the reactor and the first loop. As shown in figure 7(*b*), the cost of the reactor accounts for 85.79% of the system. The fusion device is the key to the price of fusion power generation. The cost of the HSL is comparable to that

**Table 8.** Exergy and economic results of the CFETR system.

| Component | $E_d$ (MW) | $C_d$ ($\$ h$^{-1}$) | $Z_k$ ($\$ h$^{-1}$) | $f_k$ | $r_k$ |
|---|---|---|---|---|---|
| CFETR | 27.521 | 583.0 | 36 048.2 | 1.98 | 1.40 |
| $P_{BNK}$ | 12.680 | 1651.6 | 236.9 | 0.13 | 0.58 |
| $P_{DIV}$ | 0.054 | 4.2 | 3.5 | 0.45 | 0.24 |
| HX-BNK | 19.943 | 2111.4 | 78.4 | 0.04 | 0.05 |
| Hot tank | 0.000 | 0.0 | 564.8 | 1.00 | 0.59 |
| Cold tank | 0.000 | 0.0 | 484.6 | 1.00 | 0.00 |
| HX-DIV | 18.137 | 1871.6 | 45.0 | 0.02 | 0.73 |
| CS | 0.000 | 17 416.0 | 1552.5 | 0.08 | 0.00 |
| $P_L$ | 0.003 | 0.1 | 0.4 | 0.74 | 1.00 |
| HX-HTS | 4.609 | 1256.2 | 46.8 | 0.04 | 0.03 |
| HX-LTS | 4.809 | 1651.8 | 26.8 | 0.02 | 0.13 |
| $T$ | 8.781 | 1084.1 | 2474.4 | 0.70 | 0.13 |
| $C$ | 4.510 | 121.6 | 289.7 | 0.70 | 0.28 |
| HTR | 5.651 | 8277.4 | 73.5 | 0.01 | 0.06 |
| LTR | 2.760 | 4042.7 | 73.6 | 0.02 | 0.05 |
| PC | 6.644 | 9732.1 | 16.6 | 0.00 | 0.27 |
| $P_{cool}$ | 0.031 | 0.5 | 2.2 | 0.81 | 0.49 |

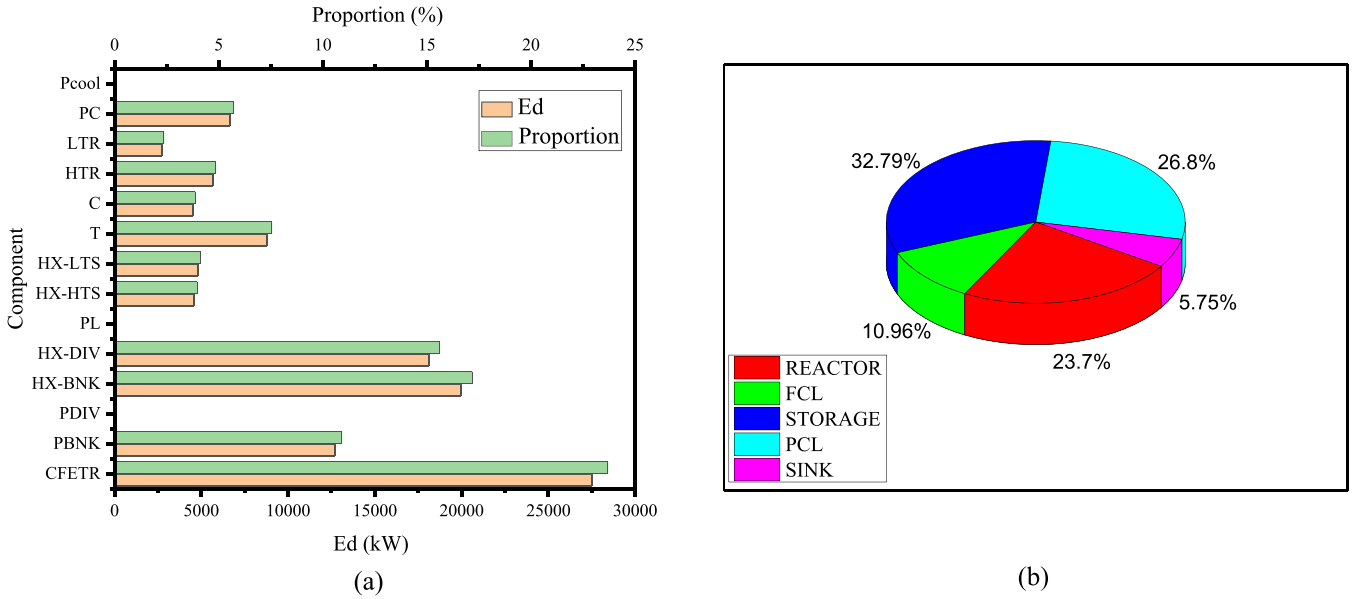


**Figure 6.** Exergy destruction rates and destruction ratios for different components of the CFETR power conversion system with new $SCO_2$ Brayton cycle.

of the PCL. In the HSL, the heat storage tank is the largest investment, accounting for about 6% of the total system cost. The turbine is the largest cost item in the PCL, accounting for nearly 6% of the total system cost, followed by the compressor for 0.7%. The SL, which includes only the heat exchanger and pump, has the smallest cost, less than 0.1% of the total system cost (cooling towers are not included).

### 3.3. Sensitivity analyses

In order to verify the system optimization results and to better understand the influence of system parameters, the sensitivity analyses on the performance of the CFETR power conversion system are studied. The key variables include the hot molten salt temperature $T_{H1}$, the flow split ratio, the MC outlet pressure $p_H$ and the MC inlet pressure $p_L$. The system performance includes the PCL thermal efficiency $\eta_{cy}$, the system exergy efficiency $\eta_{ex}$ and the total system product unit cost $cp_{tot}$. When analyzing the effect of any variable, other variables remain constant. The optimization variables are selected in the interval shown in equation (22), and some cases are abandoned because they do not meet the limitation of the heat source parameters shown in table 1.

Figure 8 depicts the sensitivity analyses of the simple $SCO_2$ Brayton cycle. Figure 8(*a*) shows the function of cycle thermal efficiency, system exergy efficiency and total system product unit cost with the molten salt temperature $T_{H1}$. The difference between the hot molten salt and the turbine inlet temperature is assumed to maintain 15 °C. With the increase of hot molten salt temperature from 410 °C to 465 °C, the

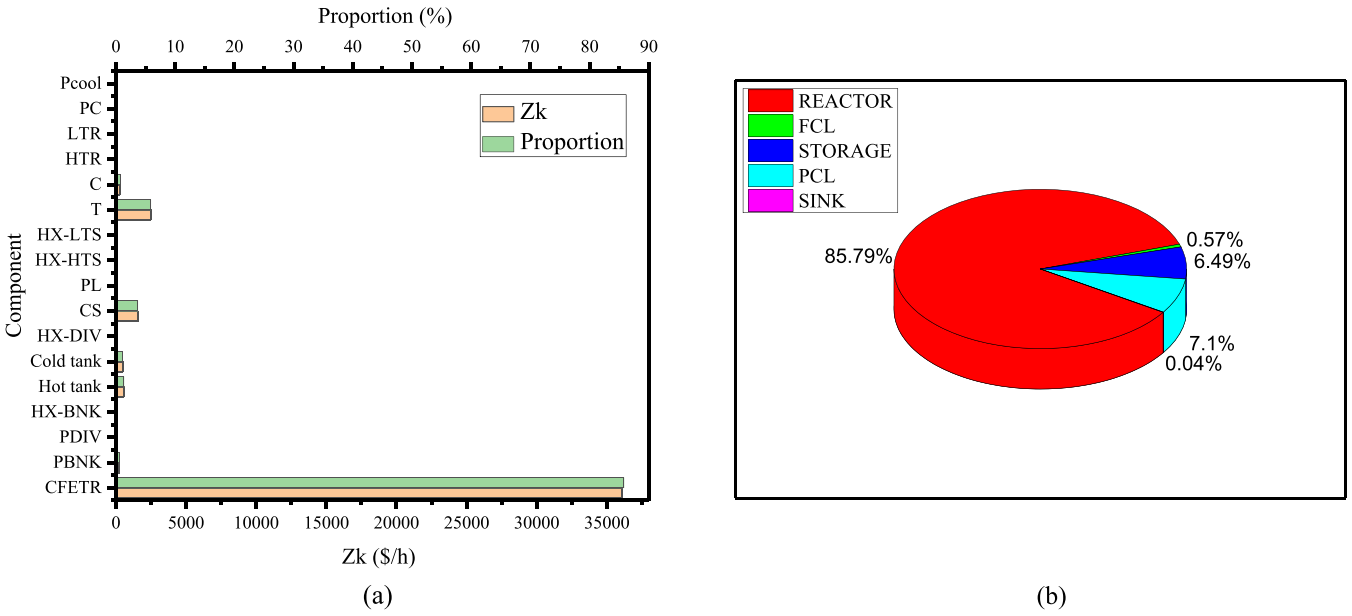


**Figure 7.** Fixed investment and maintenance costs for different components of CFETR power conversion system with new $SCO_2$ Brayton cycle.

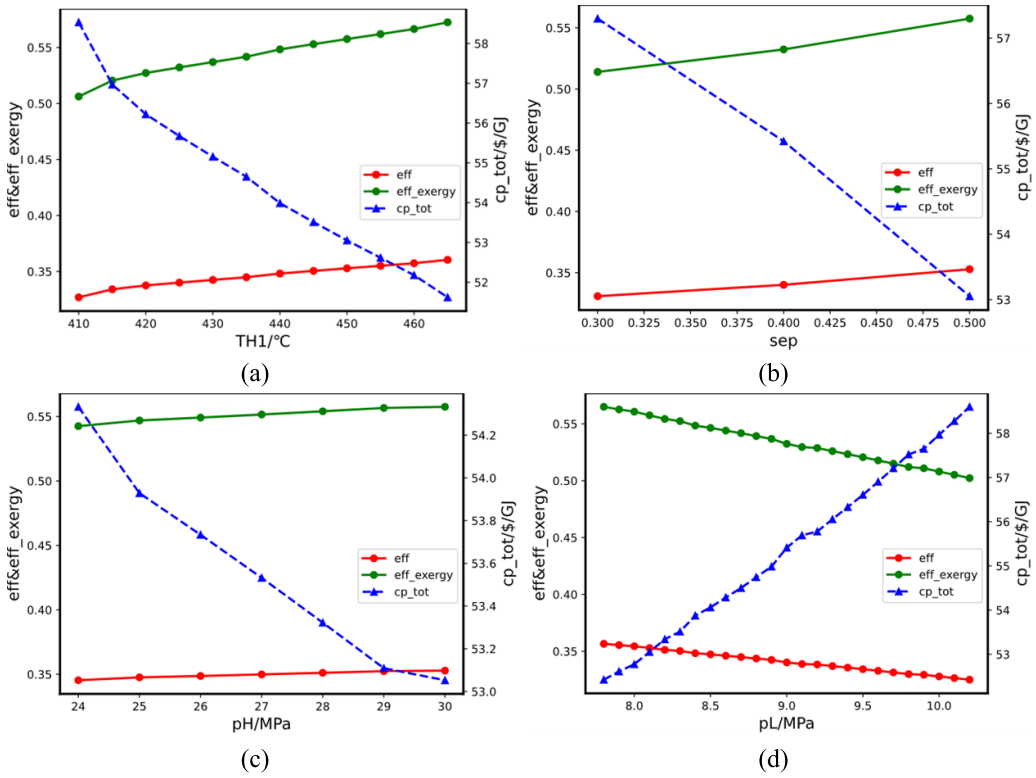


**Figure 8.** Sensitivity analyses of simple $SCO_2$ Brayton cycle system.

cycle thermal efficiency becomes greater due to the increase of the heat recovery in PCL, the system exergy efficiency increases and the total system product unit cost decreases. Figure 8(*b*) reflects the variation of fitness functions with the flow split ratios. As is shown, the split ratios can vary only within a certain range. The larger the split ratio, the stronger the heat recovery capacity. The maximum split ratio corresponds to the maximum efficiency and the lowest cost. Figure 8(*c*) shows the effect of the MC outlet pressure. As the pressure increases, the turbine power increases and the net power increases. Therefore, the thermal efficiency and the exergy efficiency increase, and the cost decreases. Figure 8(*d*) shows the effect of the MC inlet pressure. The maximum thermal efficiency is reached at around 7.8 MPa. The higher the pressure, the lower the efficiency and the higher the cost.

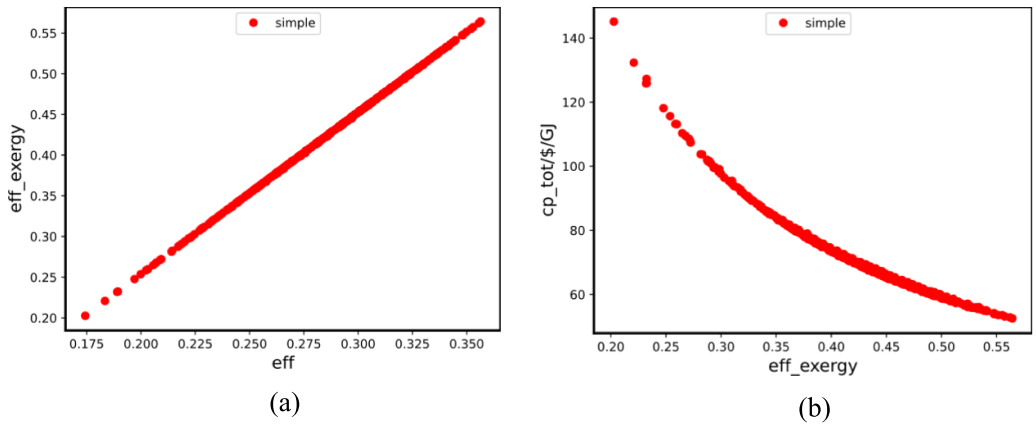


**Figure 9.** Function of fitness functions.

**Table 9.** Optimal operating parameters obtained by multi-criteria optimization of weighting.

| Cycle | $T_{H1}$ (°C) | *Sep* | $p_H$ (MPa) | $p_L$ (MPa) | $T_{L6}$ (°C) | $T_{H2}$ (°C) | $\eta_{gross}$ | $\eta_{ex}$ | $cp_{tot}$ ($ GJ$^{-1}$) |
|---|---|---|---|---|---|---|---|---|---|
| Simple (BNK + DIV) | 438.3 | 0.64 | 24.4 | 7.9 | 184.9 | 285.0 | 37.4% | 59.8% | 49.64 |

**Table 10.** Optimal operating parameters obtained by multi-criteria optimization of weighting under parameter limitations.

| Cycle | $T_{H1}$ (°C) | *Sep* | $p_H$ (MPa) | $p_L$ (MPa) | $T_{L6}$ (°C) | $T_{H2}$ (°C) | $\eta_{gross}$ | $\eta_{ex}$ | $cp_{tot}$/$/GJ |
|---|---|---|---|---|---|---|---|---|---|
| Simple (BNK + DIV) | 436.3 | 0.64 | 23.3 | 7.7 | 182.4 | 285.0 | 37.0% | 59.2% | 50.19 |

In the sensitivity analyses, the hot molten salt temperature has the greatest effect on the system power generation performance, the split ratio and MC inlet pressure are also critical, while the influence of MC outlet pressure is relatively small. Meanwhile, the optimal variable values obtained from the sensitivity analyses verify the previous results in table 6.

### 3.4. Multi-criteria optimization

The exergy, exergoeconomic and sensitivity analyses of the CFETR power conversion system with the new $SCO_2$ Brayton cycle have been performed, respectively. As mentioned above, there are multiple important variables such as hot molten salt temperature, flow split ratio of PCL, MC outlet pressure, MC inlet pressure, as well as multiple optimization fitness functions such as PCL thermal efficiency, the system exergy efficiency, the total system product unit cost in the present power system. Therefore, multi-criteria optimization is studied in this section, and the results based on different algorithms can be mutually validated.

With the BF algorithm, the variables are taken within the interval of equation (22), and multiple values of the four variables are arbitrarily arranged and combined. The scatter diagrams of the relationship between PCL thermal efficiency and system exergy efficiency, and the relationship between system exergy efficiency and total system product unit cost, are shown in figure 9. The trend obtained for the new power conversion system shows that PCL thermal efficiency changes synchronously with the system exergy efficiency, indicating that the internal consumption of the power plant has little impact on power generating. The total system product unit cost decreases with the increase in the system exergy efficiency. In addition, we also used the multi-criteria GA for the three fitness functions' optimization to obtain the Pareto front, and the results focus on one point as detailed in figure A1, which also shows that the maximum efficiency and the minimum cost can be obtained simultaneously.

Finally, the approximate optimization of the method of weighting is used to obtain the fitness functions for comparison. Table 9 summarizes the corresponding variables and fitness functions when the above multi-criteria function $f$ in equation (25) is maximized. The optimal variables and the optimal fitness functions are consistent with table 6. Considering the restrictions of material processing shown in equation (23), the optimization parameter range is narrowed, and the obtained optimal results are shown in table 10.

## 4. Conclusion

In this paper, several $SCO_2$ Brayton cycle configurations with different arrangements of dual heat sources, BNK and DIV, were studied. A new $SCO_2$ Brayton cycle for the CFETR power conversion system was developed. Comprehensive research has been carried out relating to the new CFETR power generation system from the perspective of thermodynamics, exergy efficiency and exergoeconomics. And several multi-criteria optimization methods were also adopted to obtain the optimal operation variable scheme. The main conclusions are as follows:

(1) The simple $SCO_2$ Brayton cycle with flow split is most suitable for the CFETR BNK/DIV dual heat sources power

conversion system due to its high thermal efficiency and simplicity.

(2) The exergy destruction of the system occurs mainly in the fusion reactor, interloop heat exchangers and turbine. And the investment and maintenance costs are mainly from the reactor, heat storage tank and turbine.

(3) The sensitivity analyses show that the hot molten salt temperature has the greatest impact on the system exergy efficiency. Increasing the hot molten salt temperature can effectively reduce the total system product unit cost.

(4) The system optimal operation variables are obtained by both the Pareto front and the method of weighting. The optimal PCL thermal efficiency, system exergy efficiency and total system product unit cost are 37.0 %, 59.2 % and 50.2 % $GJ^{-1}$, respectively.

## Acknowledgments

This work is financially supported by the Fundamental Research Funds for the Central Universities Grant No. WK214000013, the National Natural Science Foundation of China under Contract No. 12075278, the National Key R&D Program of China under Contract No. 2017YFE0300604. The numerical calculations in this paper have been conducted on the supercomputing system in the Supercomputing Center of the University of Science and Technology of China (USTC).

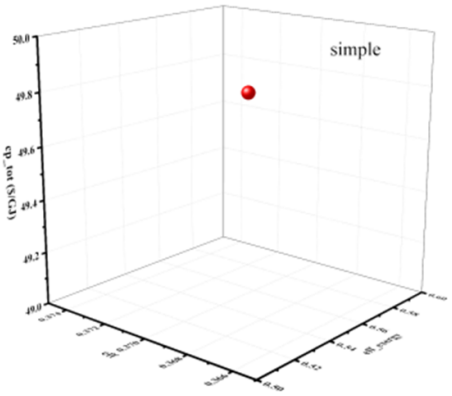


**Figure A1.** Distribution of Pareto front.

## Appendix

The Pareto front for multi-criteria optimization is shown in figure A1. The Pareto front presents the optimal solution under the three fitness functions. The optimal solution shows a difference of only five decimal places, so they can be considered the same. Therefore, the Pareto front degenerates to one point, so the maximum cycle thermal efficiency, the maximum system exergy efficiency and the lowest total system product unit cost can be achieved simultaneously under the optimal variables.

**Table A1.** Nomenclature.

| | | | |
|---|---|---|---|
| $SCO_2$ | Supercritical carbon dioxide | $q$ | Mass flow rate (kg $s^{-1}$) |
| PCL | Power conversion loop | $e$ | Exergy per unit mass flow (kJ $kg^{-1}$) |
| CFETR | Chinese fusion engineering testing reactor | $c$ | Cost rate per unit mass flow (\$ $kg^{-1}$) |
| BNK | Blanket | $cp$ | Product unit cost (\$ $GJ^{-1}$) |
| DIV | Divertor | $c_p$ | Isobaric specific heat capacity (J (kg·K) $^{-1}$) |
| ITER | International tokamak experimental reactor | $sep$ | Split ratio |
| DEMO | DEMOnstration power plant | $n$ | Anticipated life time |
| FCL | First cooling loop | $i$ | Interest rate |
| GA | Genetic algorithm | $r$ | Relative cost difference |
| HX-HTS | Heat exchanger between molten salt storage loop and PCL | $f$ | Exergoeconomic factor |
| HX-LTS | Heat exchanger between concrete storage loop and PCL | *Simple* | Simple $SCO_2$ Brayton cycle |
| HX-BNK | Heat exchanger between molten salt storage loop and FCL | $\Delta p$ | Pressure drop |
| HX-BNK | Heat exchanger between concrete storage loop and FCL | $\tau$ | Annual operating hours |
| PC | Pre-cooler | $\varepsilon$ | Component isentropic efficiency |
| MC | Main compressor | $\rho$ | Local density of the fluid (kg $m^{-3}$) |
| AC | Auxiliary compressor | $\eta$ | Cycle efficiency |
| LTR | Low temperature recuperator | $\phi$ | Maintenance factor |
| HTR | High temperature recuperator | $\kappa$ | Generator efficiency |
| T | Turbine | | |
| P | Pump | **Subscript** | |
| PCHE | Printed circuit heat exchanger | F | Fuel |
| PEC | Capital cost (\$) | P | Product |
| CEPCI | Chemical engineering plant cost index | H | Molten salt storage loop |
| CRF | Capital recovery factor | L | Concrete storage loop |
| SPECO | Specific exergy costing | D/DIV | First cooling loop of DIV |
| GTC | Gas turbine cycle | B/BNK | First cooling loop of BNK |
| ORC | Organic Rankine cycle | C/COOL | Sink loop |
| ARC | Absorption refrigeration cycle | T | Turbine |
| HSL | Heat storage loop | d | Destruction |
| SL | Sink loop | q | Heat |
| IC | Inter-cooling compressor | 0 | Ambient temperature |
| SEP | Separator | salt | Molten salt heat storage loop |
| MIX | Mixture | fuel | Fuel into system |
| $W$ | Power (kW) | c | Compressor |
| $Q$ | Heat from heat source (kW) | in | Inlet |
| $T$ | Temperature (°C) | out | Outlet |
| $E$ | Exergy (kW) | cy | Power conversion cycle |
| $C$ | Cost rate (\$ $h^{-1}$) | gross | Electric |
| $Z_k$ | Cost rate associated with capital investment, operation and maintenance expenses for the $k$th component (\$ $h^{-1}$) | e | Net thermodynamic (efficiency) |
| $A$ | Heat exchanger area ($m^2$) | ex | Exergy |
| $H$ | Enthalpy (kW $kg^{-1}$) | r | Reheat $SCO_2$ Brayton cycle |
| s | Entropy (kW $(kgK)^{-1}$) | c | Two-stage $SCO_2$ Brayton Cycle with intermediate cooling |
| $p$ | Pressure | tot | Whole system |
| $p_H$ | Highest pressure in PCL | max | Maximum value |
| $p_L$ | Lowest pressure in PCL | min | Minimum value |

**Table A2.** Detailed calculation equations for work of turbomachinery and pump power of each loop.

| Component | Work |
|---|---|
| Turbine | $q_{10}(h_9\text{-}h_{10})\varepsilon_T$ |
| Compressor | $q_1(h_2\text{-}h_1)\varepsilon_c$ |
| $p_{BNK}$ | $q_{B1}(h_{B1}\text{-}h_{B3})\varepsilon_p$ |
| $p_{DIV}$ | $q_{D1}(h_{D1}\text{-}h_{D3})\varepsilon_p$ |
| $p_L$ | $q_{L1}(h_{L1}\text{-}h_{L3})\varepsilon_p$ |
| $p_{sink}$ | $q_{C1}(h_{C1}\text{-}h_{C3})\varepsilon_p$ |

**Table A3.** Simple Brayton cycle and recompression Brayton cycle calculation model validation.

| | 37.34%[a] | | Validation 37.28% | | 40.59%[b] | | Validation 40.58% | |
|---|---|---|---|---|---|---|---|---|
| Efficiency | Temperature | Pressure | Temperature | Pressure | Temperature | Pressure | Temperature | Pressure |
| 1 | 451.1 | 300 | 451.1 | 300 | 446.5 | 280 | 446.5 | 280 |
| 2 | 309.1 | 85.8 | 309.1 | 85.8 | 313 | 86.2 | 313 | 86.2 |
| 3 | 81.6 | 85.4 | 81.9 | 85.4 | 169.9 | 85.8 | 169.9 | 85.8 |
| 4 | 35 | 85 | 35 | 85 | 65.2 | 85.4 | 65.3 | 85.4 |
| 5 | 76.6 | 300.8 | 76.6 | 300.8 | 65.2 | 85.4 | 65.3 | 85.4 |
| 6 | 76.6 | 300.8 | 76.6 | 300.8 | 65.2 | 85.4 | 65.3 | 85.4 |
| 7 | 304.1 | 300.4 | 304.1 | 300.4 | 30 | 85 | 30 | 85 |
| 8 | 76.6 | 300.8 | 76.6 | 300.8 | 58.2 | 281.2 | 58.3 | 281.2 |
| 9 | 131.3 | 300.4 | 131.3 | 300.4 | 172.2 | 280.8 | 172.4 | 280.8 |
| 10 | 252.4 | 300.4 | 252.1 | 300.4 | 162.9 | 280.4 | 162.2 | 280.4 |
| 11 | | | | | 165.9 | 280.8 | 165.9 | 280.8 |
| 12 | | | | | 278 | 280.4 | 278 | 280.4 |
| 13 | | | | | 58.2 | 281.2 | 58.3 | 281.2 |
| 14 | | | | | 58.2 | 281.2 | 58.3 | 281.2 |
| 15 | | | | | 78.4 | 280.8 | 79.3 | 280.8 |
| 16 | | | | | 172.2 | 280.4 | 178.6 | 280.4 |

[a] [23].
[b] [13].

**Table A4.** Exegetic fuel and product and associated cost rates for each component.

| Component | Exergetic fuel (MW) $E_F$ | Exergetic product (MW) $E_P$ | Exergy destruction (MW) $E_d$ | Associated cost of fuel ($ h$^{-1}$) $C_F$ | Associated cost of product ($ h$^{-1}$)$C_P$ |
|---|---|---|---|---|---|
| BNK | $E_{BNK}$ | $q_{B2}(E_{B2}\text{-}E_{B1})$ | $E_{BNK}\text{-}q_{B2}(E_{B2}\text{-}E_{B1})$ | $C_{fuelBNK}$ | $C_{B2}\text{-}C_{B1}$ |
| $P_{BNK}$ | $W_{PBNK}$ | $q_{B2}(E_{B1}\text{-}E_{B3})$ | $W_{PBNK}\text{-}q_{B2}(E_{B1}\text{-}E_{B3})$ | $C_{WPBNK}$ | $C_{B1}\text{-}C_{B3}$ |
| DIV | $E_{DIV}$ | $q_{D2}(E_{D2}\text{-}E_{D1})$ | $E_{DIV}\text{-}q_{D2}(E_{D2}\text{-}E_{D1})$ | $C_{fuelDIV}$ | $C_{D2}\text{-}C_{D1}$ |
| $P_{DIV}$ | $W_{PDIV}$ | $q_{D1}(E_{D1}\text{-}E_{D3})$ | $W_{PDIV}\text{-}q_{D2}(E_{D1}\text{-}E_{D3})$ | $C_{WPDIV}$ | $C_{D1}\text{-}C_{D3}$ |
| HX-BNK | $q_{B2}(E_{B2}\text{-}E_{B3})$ | $q_{H5}(E_{H5}\text{-}E_{H4})$ | $q_{B2}(E_{B2}\text{-}E_{B3})\text{-}q_{H5}(E_{H5}\text{-}E_{H4})$ | $C_{B2}\text{-}C_{B3}$ | $C_{H5}\text{-}C_{H4}$ |
| Hot tank | $q_{H5}E_{H5}$ | $q_{H1}E_{H1}$ | $q_{H5}E_{H5}\text{-}q_{H1}E_{H1}$ | $C_{H5}$ | $C_{H1}$ |
| Cold tank | $q_{H2}E_{H2}$ | $q_{H3}E_{H3}$ | $q_{H2}E_{H2}\text{-}q_{H3}E_{H3}$ | $C_{H2}$ | $C_{H3}$ |
| HX-DIV | $q_{D2}(E_{D2}\text{-}E_{D3})$ | $q_{L2}(E_{L2}\text{-}E_{L1})$ | $q_{D2}(E_{D2}\text{-}E_{D3})\text{-}q_{L2}(E_{L2}\text{-}E_{L1})$ | $C_{D2}\text{-}C_{D3}$ | $C_{L2}\text{-}C_{L1}$ |
| CS | $q_{L2}E_{L2}$ | $q_{L3}E_{L3}$ | $q_{L2}E_{L2}\text{-}q_{L3}E_{L3}$ | $C_{L2}$ | $C_{L3}$ |
| $P_L$ | $W_{PL}$ | $q_{L1}(E_{L1}\text{-}E_{L3})$ | $W_{PL}\text{-}q_{L1}(E_{L1}\text{-}E_{L3})$ | $C_{WPL}$ | $C_{L1}\text{-}C_{L3}$ |
| HX-HTS | $q_{H1}(E_{H1}\text{-}E_{H2})$ | $q_9(E_9\text{-}E_8)$ | $q_{H1}(E_{H1}\text{-}E_{H2})\text{-}q_9(E_9\text{-}E_8)$ | $C_{H1}\text{-}C_{H2}$ | $C_9\text{-}C_8$ |
| HX-LTS | $q_{L6}(E_{L6}\text{-}E_{L3})$ | $q_6(E_6\text{-}E_4)$ | $q_{H1}(E_{L6}\text{-}E_{L3})\text{-}q_6(E_6\text{-}E_4)$ | $C_{L6}\text{-}C_{L3}$ | $C_6\text{-}C_4$ |
| T | $q_9(E_9\text{-}E_{10})$ | $W_T$ | $q_9(E_9\text{-}E_{10})\text{-}W_T$ | $C_9\text{-}C_{10}$ | $C_{WT}$ |
| C | $W_C$ | $q_2(E_2\text{-}E_1)$ | $W_C\text{-}q_2(E_2\text{-}E_1)$ | $C_{WC}$ | $C_2\text{-}C_1$ |
| HTR | $q_{10}(E_{10}\text{-}E_{11})$ | $q_8(E_8\text{-}E_7)$ | $q_{10}(E_{10}\text{-}E_{11})\text{-}q_8(E_8\text{-}E_7)$ | $C_{10}\text{-}C_{11}$ | $C_8\text{-}C_7$ |
| LTR | $q_{11}(E_{11}\text{-}E_{12})$ | $q_5(E_5\text{-}E_3)$ | $q_{11}(E_{11}\text{-}E_{12})\text{-}q_3(E_5\text{-}E_3)$ | $C_{11}\text{-}C_{12}$ | $C_5\text{-}C_3$ |
| PC | $q_{12}(E_{12}\text{-}E_1)$ | $q_{C2}(E_{C2}\text{-}E_{C1})$ | $q_{12}(E_{12}\text{-}E_1)\text{-}q_{C2}(E_{C2}\text{-}E_{C1})$ | $C_{12}\text{-}C_1$ | $C_{C2}\text{-}C_{C1}$ |
| $P_{cool}$ | $W_{Pcool}$ | $q_{C1}(E_{C1}\text{-}E_{C3})$ | $W_{Pcool}\text{-}q_{C1}(E_{C1}\text{-}E_{C3})$ | $C_{WPcool}$ | $C_{C1}\text{-}C_{C3}$ |

**Table A5.** Exergoeconomic costing and auxiliary equations for the CFETR system.

| Component | Costing balance equations | Auxiliary equations |
|---|---|---|
| BNK | $C_{B2} = C_{B1} + Z_{BNK} + C_{fuelBNK}$ | $C_{B2}/E_{B2} = C_{B1}/E_{B1}$ |
| $P_{BNK}$ | $C_{B1} = C_{B3} + Z_{PBNK} + C_{WPBNK}$ | $C_{B3}/E_{B3} = C_{B1}/E_{B1}$ |
| DIV | $C_{D2} = C_{D1} + Z_{DIV} + C_{fuelDIV}$ | $C_{D2}/E_{D2} = C_{D1}/E_{D1}$ |
| $P_{DIV}$ | $C_{D1} = C_{D3} + Z_{PDIV} + C_{WPDIV}$ | $C_{D3}/E_{D3} = C_{D1}/E_{D1}$ |
| HX-BNK | $C_{B3} + C_{H5} = C_{H4} + C_{B2} + Z_{HX\text{-}BNK}$ | |
| Hot tank | $C_{H1} = C_{H5} + Z_{HOT}$ | |
| Cold tank | $C_{H3} = C_{H2} + Z_{COLD}$ | $C_{H1}/E_{H1} = C_{H2}/E_{H2}$ |
| HX-DIV | $C_{D3} + C_{L2} = C_{L1} + C_{D2} + Z_{HX\text{-}DIV}$ | $C_{L3}/E_{L3} = C_{L4}/E_{L4}$ |
| *CS* | $C_{L3} = C_{L2} + Z_{CON}$ | $C_{L2}/E_{L2} = C_{L5}/E_{L5} = C_{L6}/E_{L6}$ |
| $P_L$ | $C_{L1} = C_{L3} + Z_{PL} + C_{WPL}$ | $C_{WPL}/E_{WPL} = C_{WPDIV}/E_{WPDIV}$ |
| HX-HTS | $C_{H2} + C_9 = C_{H1} + C_8 + Z_{HX\text{-}HTS}$ | $C_{WT}/E_{WT} = C_{WPDIV}/E_{WPDIV}$ |
| HX-LTS | $C_{L3} + C_6 = C_{L6} + C_4 + Z_{HX\text{-}LTS}$ | $C_{WC}/E_{WC} = C_{WPDIV}/E_{WPDIV}$ |
| *T* | $C_{10} + C_{WT} = C_9 + Z_T$ | $C_7 = C_5 + C_6$ |
| *C* | $C_2 = C_1 + C_{WC} + Z_C$ | $C_2 = C_3 + C_4$, $sepC_2 = C_3$ |
| HTR | $C_{11} + C_8 = C_7 + C_{10} + Z_{HTR}$ | $C_1/E_1 = C_{12}/E_{12}$ |
| LTR | $C_5 + C_{12} = C_3 + C_{11} + Z_{LTR}$ | $C_{10}/E_{10} = C_{11}/E_{11} = C_{12}/E_{12}$ |
| PC | $C_1 + C_{C2} = C_{12} + C_{C1} + Z_{PC}$ | $C_{WPcool}/E_{WPcool} = C_{WPDIV}/E_{WPDIV}$ |
| $P_{cool}$ | $C_{C1} = C_{WPcool} + C_{C3} + Z_{Pcool}$ | $C_{C2}/E_{C2} = C_{C3}/E_{C3}$ |

## ORCID iDs

Ke Liu https://orcid.org/0000-0002-2192-227X
Mingzhun Lei https://orcid.org/0000-0002-8436-1000
Changhong Peng https://orcid.org/0000-0003-0368-9301

## References

[1] Ongena J. and Oost G.V. 2012 Energy for future centuries: prospects for fusion power as a future energy source *Fusion Sci. Technol.* **61** 3–16
[2] Zhuang G. *et al* 2019 Progress of the CFETR design *Nucl. Fusion* **59** 112010
[3] Alali A.E. and Al-Shboul K.F. 2018 Performance analysis of the closed Brayton power cycle in a small-scale pebble bed gas cooled reactor using different working fluids *Ann. Nucl. Energy* **121** 316–23
[4] Ishiyama S., Muto Y., Kato Y., Nishio S., Hayashi T. and Nomoto Y. 2008 Study of steam, helium and supercritical $CO_2$ turbine power generations in prototype fusion power reactor *Prog. Nucl. Energy* **50** 325–32
[5] Stepanek J., Entler S., Syblik J., Vesely L., Dostal V. and Zacha P. 2021 Comprehensive comparison of various working media and corresponding power cycle layouts for the helium-cooled DEMO reactor *Fusion Eng. Des.* **166** 112287
[6] Linares J.I., Herranz L.E., Moratilla B.Y. and Serrano I.P. 2011 Power conversion systems based on Brayton cycles for fusion reactors *Fusion Eng. Des.* **86** 2735–8
[7] Dupre J.B. 2020 Sustainable energy for scientific antarctic stations: development of a concept power plant using a small modular reactor coupled with a supercritical $CO_2$ Brayton cycle Pontificia Universidad Catolica de Chile *0640: Sustainability 0756: Nuclear physics 0791: Energy* Pontificia Universidad Catolica de Chile
[8] Kong F., Li Y., Sa R., Bai Y., Jin M. and Song Y. 2019 Design and thermodynamic analysis of supercritical $CO_2$ reheating recompression Brayton cycle coupled with lead-based reactor *Int. J. Energy Res.* **43** 4940–8
[9] Wu P., Gao C., Huang Y., Zhang D. and Shan J. 2020 Supercritical $CO_2$ Brayton cycle design for small modular reactor with a thermodynamic analysis solver *Sci. Technol. Nucl. Install.* **2020** e5945718
[10] Syblik J., Vesely L., Entler S., Stepanek J. and Dostal V. 2019 Analysis of supercritical $CO_2$ Brayton power cycles in nuclear and fusion energy *Fusion Eng. Des.* **146** 1520–3
[11] Serrano I.P., Linares J.I., Cantizano A. and Moratilla B.Y. 2014 Enhanced arrangement for recuperators in supercritical $CO_2$ Brayton power cycle for energy conversion in fusion reactors *Fusion Eng. Des.* **89** 1909–12
[12] Serrano I.P., Linares J.I., Cantizano A. and Moratilla B.Y. 2013 A novel supercritical $CO_2$ power cycle for energy conversion in fusion power plants *Fusion Sci. Technol.* **64** 483–7
[13] Linares J.I., Herranz L.E., Fernández I., Cantizano A. and Moratilla B.Y. 2015 Supercritical $CO_2$ Brayton power cycles for DEMO fusion reactor based on helium cooled lithium lead blanket *Appl. Therm. Eng.* **76** 123–33
[14] Chen Z., Wan T., Zhao P., Lei M. and Li Y. 2021 Study of power conversion system for Chinese fusion engineering testing reactor *Energy* **218** 119495
[15] Zahedi R., Ahmadi A. and Dashti R. 2021 Energy, exergy, exergoeconomic and exergoenvironmental analysis and optimization of quadruple combined solar, biogas, SRC and ORC cycles with methane system *Renew. Sustain. Energy Rev.* **150** 111420
[16] Wang S., Liu C., Li J., Sun Z., Chen X. and Wang X. 2020 Exergoeconomic analysis of a novel trigeneration system containing supercritical $CO_2$ Brayton cycle, organic Rankine cycle and absorption refrigeration cycle for gas turbine waste heat recovery *Energy Convers. Manage.* **221** 113064
[17] Al-Rashed A.A.A.A. and Afrand M. 2021 Multi-criteria exergoeconomic optimization for a combined gas turbine-supercritical $CO_2$ plant with compressor intake cooling fueled by biogas from anaerobic digestion *Energy* **223** 119997
[18] Guelpa E. and Verda V. 2020 Exergoeconomic analysis for the design improvement of supercritical $CO_2$ cycle in concentrated solar plant *Energy* **206** 118024
[19] Liu Z., Liu Z., Cao X., Luo T. and Yang X. 2020 Advanced exergoeconomic evaluation on supercritical carbon dioxide recompression Brayton cycle *J. Clean Prod.* **256** 120537

[20] Du Y., Yang C., Hu C. and Zhang C. 2021 Thermoeconomic analysis and inter-stage pressure ratio optimization of nuclear power supercritical $CO_2$ multi-stage recompression *Int. J. Energy Res.* **45** 2367–82

[21] Luo D. and Huang D. 2020 Thermodynamic and exergoeconomic investigation of various $SCO_2$ Brayton cycles for next generation nuclear reactors *Energy Convers. Manage.* **209** 112649

[22] Wei S., Sun X., Wang H., Jia J., Chen Z. and Zhang S. 2020 Preliminary safety analysis of tritium source term for the CFETR tritium plant *Fusion Sci. Technol.* **76** 869–77

[23] Linares J.I., Arenas E., Cantizano A., Porrasa J., Moratilla B.Y., Carmona M. and Batet L. 2018 Sizing of a recuperative supercritical $CO_2$ Brayton cycle as power conversion system for DEMO fusion reactor based on dual coolant lithium lead blanket *Fusion Eng. Des.* **134** 79–91

[24] Alva G., Lin Y. and Fang G. 2018 An overview of thermal energy storage systems *Energy* **144** 341–78

[25] Alonso M.C., Vera-Agullo J., Guerreiro L., Flor-Laguna V., Sanchez M. and Collares-Pereira M. 2016 Calcium aluminate based cement for concrete to be used as thermal energy storage in solar thermal electricity plants *Cem. Concr. Res.* **82** 74–86

[26] Zhang D., Cui S., Cheng J., Tian W. and Su G.H. 2018 Improving the optimization algorithm of NTCOC for application in the HCSB blanket for CFETR phase II *Fusion Eng. Des.* **135** 216–27

[27] Peng X., Liu P., Lu K., Qin S., Mao X. and Qian X. 2020 Design optimization of plasma facing unit fixation distribution for CFETR divertor *Fusion Eng. Des.* **152** 111434

[28] Qin S. *et al* 2020 Preliminary design progress of the CFETR water-cooled divertor *IEEE Trans. Plasma Sci.* **48** 1733–42

[29] Wu P., Ma Y., Gao C., Liu W., Shan J., Huang Y., Wang J., Zhang D. and Ran X. 2020 A review of research and development of supercritical carbon dioxide Brayton cycle technology in nuclear engineering applications *Nucl. Eng. Des.* **368** 110767

[30] Liu Y., Wang Y. and Huang D. 2019 Supercritical $CO_2$ Brayton cycle: a state-of-the-art review *Energy* **189** 115900

[31] Bejan A. 1995 *Thermal Design and Optimization* (Hoboken, NJ: Wiley)

[32] Lazzaretto A. and Tsatsaronis G. 2006 SPECO: a systematic and general methodology for calculating efficiencies and costs in thermal systems *Energy* **31** 1257–89

[33] Wang X. and Dai Y. 2016 Exergoeconomic analysis of utilizing the transcritical $CO_2$ cycle and the ORC for a recompression supercritical $CO_2$ cycle waste heat recovery: a comparative study *Appl. Energy* **170** 193–207

[34] Ma Y., Morozyuk T., Liu M., Yan J. and Liu J. 2019 Optimal integration of recompression supercritical $CO_2$ Brayton cycle with main compression intercooling in solar power tower system based on exergoeconomic approach *Appl. Energy* **242** 1134–54

[35] Oishi T., Yamazaki K., Arimoto H., Ban K., Kondo T., Tobita K. and Goto T. 2012 Comparative study of cost models for tokamak DEMO fusion reactors *Plasma Fusion Res.* **7** 2405115

[36] Hender T.C., Knight P.J. and Cook I. 1996 Key issues for the economic viability of magnetic fusion power *Fusion Technol.* **30** 1605–12

[37] Siegbahn K. and Karlsson E. 1986 *Nuclear Instruments and Methods in Physics Research. Section A: Accelerators, Spectrometers, Detectors and Associated Equipment* vol A249 (Columbia: Missouri Univ.)

[38] Fahroni M.A., Pratiwi D., Romadhoni A. and Syambas N.R. 2021 Brute force modification algorithm for ring topology network optimization *2021 15th Int. Conf. on Telecommunication Systems, Services, and Applications (TSSA)* (*Bali, Indonesia*, *18–19 November 2021*) (TSSA) pp 1–5

[39] Lambora A., Gupta K. and Chopra K. 2019 Genetic algorithm-a literature review (*Faridabad, India*, *14–16 February 2019*) *2019 Int. Conf. on Machine Learning, Big Data, Cloud and Parallel Computing (Comitcon)* pp 380–4

[40] Vandani A.M.K., Bidi M. and Ahmadi F. 2015 Exergy analysis and evolutionary optimization of boiler blowdown heat recovery in steam power plants *Energy Convers. Manage.* **106** 1–9

[41] Mohagheghi M., Kapat J. and Nagaiah N. 2014 Pareto-based multi-objective optimization of recuperated S-CO2 Brayton cycles *ASME Turbo Expo 2014: Turbine Technical Conference and Exposition* vol 45660 (Dusseldorf: American Society of Mechanical Engineers Digital Collection) p V03BT36A018

[42] Wang K. and He Y.-L. 2017 Thermodynamic analysis and optimization of a molten salt solar power tower integrated with a recompression supercritical $CO_2$ Brayton cycle based on integrated modeling *Energy Convers. Manage.* **135** 336–50

[43] Rozman K.A., Saranam V.R., Doğan Ö.N., Paul B.K. and Hawk J.A. 2021 Effect of specimen orientation on the mechanical performance of diffusion bonded 316 stainless steel for hybrid printed circuit heat exchangers *J. Mater. Eng. Perform.* **30** 7950–7

[44] Alharbi S., Elsayed M.L. and Chow L.C. 2020 Exergoeconomic analysis and optimization of an integrated system of supercritical $CO_2$ Brayton cycle and multi-effect desalination *Energy* **197** 117225

[45] Mohagheghi M. and Kapat J. 2013 Thermodynamic optimization of recuperated S-$CO_2$ Brayton cycles for solar tower applications *ASME Turbo Expo 2013: Turbine Technical Conference and Exposition* vol 55133 (San Antonio, TX: American Society of Mechanical Engineers Digital Collection) p V002T07A013

[46] Sun L., Wang D. and Xie Y. 2021 Thermodynamic and exergoeconomic analysis of combined supercritical $CO_2$ cycle and organic Rankine cycle using $CO_2$-based binary mixtures for gas turbine waste heat recovery *Energy Convers. Manage.* **243** 114400

[47] Liu Z. and He T. 2020 Exergoeconomic analysis and optimization of a gas turbine-modular helium reactor with new organic Rankine cycle for efficient design and operation *Energy Convers. Manage.* **204** 112311

[48] Crespi F., Sánchez D., Rodríguez J.M. and Gavagnin G. 2017 Fundamental thermo-economic approach to selecting s$CO_2$ power cycles for CSP applications *Energy Proc.* **129** 963–70

[49] Stack OverflowStack Overflow *Optimization (scipy.optimize)* (available at: https://docs.scipy.org/doc/scipy/tutorial/optimize.html) (Accessed 30 April 2022)

[50] Geatpy Development Team *Geatpy – The Genetic and Evolutionary Algorithm Toolbox for Python with High Performance* (available at: http://geatpy.com/index.php/home/) (Accessed 30 April 2022)